Supplementary material for: "Quenched disorder and instability control dynamic fracture in three dimensions"

Yuri Lubomirsky[1] and Eran Bouchbinder[1]
[1] *Chemical and Biological Physics Department, Weizmann Institute of Science, Rehovot 7610001, Israel*

I. Supplementary Notes

A. A simple probabilistic model of localized branching in 3D

As explained in the manuscript, the auxiliary quenched disorder field $\zeta(\boldsymbol{x})$ is initially extracted from a Gaussian distribution of zero mean and standard deviation σ, $\frac{1}{\sqrt{2\pi}\sigma}\exp(-\frac{1}{2}\zeta^2/\bar{\sigma}^2)$, independently for each spatial location $\boldsymbol{x}$. This Gaussian probability distribution function is normalized over the domain $-\infty<\zeta<\infty$. However, we defined for a physical parameter α the following disordered field $\alpha(\boldsymbol{x})/\alpha_0 = 1+\alpha_{_\zeta}\zeta(\boldsymbol{x})$, with $0\leq\alpha_{_\zeta}\leq 1$, which can become negative for sufficiently negative values of ζ. As in our case α corresponds to the quasi-static fracture energy, which is a positive quantity, to ensure its positivity for any $\alpha_{_\zeta}$ we restrict the Gaussian distribution to be valid for $-1<\zeta<\infty$. To conform with the conservation of probability, we attribute the probability $\int_{-\infty}^{-1}\frac{1}{\sqrt{2\pi}\sigma}\exp(-\frac{1}{2}\zeta^2/\bar{\sigma}^2)\,d\zeta$ to $\zeta=-1$. This probability (corresponding to a probability density proportional to a delta-function, $\delta(\zeta+1)$) constitutes a small addition to the Gaussian distribution over $-1<\zeta<\infty$ for the σ values we considered in the manuscript. Finally, as explained above, the disordered field is convolved with a compact support kernel, endowing it with a spatial correlation length R.

This quenched disorder generation procedure is applied in the manuscript to the quasi-static fracture energy, i.e., α/α_0 is identified with $\bar{\Gamma}/\Gamma_0$. When the probability distribution $p(\bar{\Gamma}/\Gamma_0)$ in 3D is considered together with the 2D homogeneous-material branching instability, which occurs when the dimensionless crack driving force G/Γ_0 surpasses a threshold $G_{\rm B}/\Gamma_0$, a simple probabilistic model of localized branching in 3D can be constructed. The model consists of three ingredients: (i) Over a characteristic lengthscale comparable to the correlation length R, the 3D material effectively corresponds to a 2D homogeneous material. (ii) Following (i), fracture energy fluctuations of characteristic scale R can lead to 3D localized branching $G/\bar{\Gamma}>G_{\rm B}/\Gamma_0$ at a given crack driving force G. (iii) Localized branching events in 3D are largely independent of each other for $G<G_{\rm B}$.

The probability distribution of $\bar{\Gamma}/\Gamma_0$ over the correlation length R remains Gaussian, yet with a renormalized standard deviation $\bar{\sigma}(\sigma,R)<\sigma$, which one can calculate. Rearranging the inequality in (ii) to read $\bar{\Gamma}/\Gamma_0<G/G_{\rm B}$ and invoking (iii), we can use $p(\bar{\Gamma}/\Gamma_0)$ over the correlation length R to estimate the localized branching instability in 3D, $p(G;\sigma)$, as

$$p(G;\sigma)\simeq\int_{-1}^{\frac{G/G_{\rm B}-1}{\alpha_{_\zeta}}}\frac{e^{-\frac{1}{2}\zeta^2/\bar{\sigma}^2}}{\sqrt{2\pi}\bar{\sigma}}\,d\zeta+\int_{-\infty}^{-1}\frac{e^{-\frac{1}{2}\zeta^2/\bar{\sigma}^2}}{\sqrt{2\pi}\bar{\sigma}}\,d\zeta \qquad (1)$$
$$=\int_{-\infty}^{\frac{G/G_{\rm B}-1}{\alpha_{_\zeta}\bar{\sigma}}}\frac{e^{-\frac{1}{2}\eta^2}}{\sqrt{2\pi}}\,d\eta=\frac{1}{2}\left[1+\mathrm{erf}\left(\frac{G/G_{\rm B}-1}{\sigma_{_{\rm R}}}\right)\right],$$

with $\sigma_{_{\rm R}}=\sqrt{2}\,\alpha_{_\zeta}\bar{\sigma}(\sigma,R)$, as in Eq. (2) in the manuscript. For $\alpha_{_\zeta}=0.9$, $\sigma=0.25$ and $R=10\xi$ used in the manuscript, we have $\sigma_{_{\rm R}}=0.233$, employed in Fig. 4a therein.

B. A fractographic signature of crack front waves

Crack front waves (FWs) are spatiotemporal objects that propagate along moving crack fronts in 3D, featuring coupled in- and out-of-plane components [1–4]. One process by which a pair of FWs is spontaneously generated is micro-branching events [2, 3], where the out-of-plane component of each FW leaves a fractographic signature on the fracture surface. It takes the form of two linear (straight) tracks emanating from the micro-branch and forming an opening angle 2γ between them, resulting in V-shaped tracks [2, 3]. The FW velocity (in the laboratory frame of reference) $c_{_{\rm FW}}$ is related to the crack propagation velocity v according to $c_{_{\rm FW}}=v/\cos(\gamma)$, where $c_{_{\rm FW}}$ was found to be close to the Rayleigh wave-speed $c_{_{\rm R}}$, very weakly dependent on v [2–5].

In Fig. 3b in the manuscript, it is observed that isolated localized branching events in our simulations are accompanied by V-shaped tracks on the fracture surface. Our goal here is to test whether these tracks are consistent with experimental observations regarding FWs. To that aim, we present in Fig. 1 a zoom in on a few localized branching events originally shown in Fig. 3b and Fig. 3f in the manuscript, where the V-shaped tracks with an opening angle 2γ are clearly observed. We find that $\gamma\simeq 21.75^\circ$, which is essentially the same for all localized branching events analyzed (see Fig. 1). The instantaneous (not the steady state) crack propagation velocity at this point in the dynamics was $v=0.835\pm 0.015c_{\rm s}$, such that we find $c_{_{\rm FW}}=v/\cos(\gamma)=0.9c_{\rm s}\simeq 0.97c_{_{\rm R}}$, which is indeed consistent with the experimentally observed velocity of FWs.

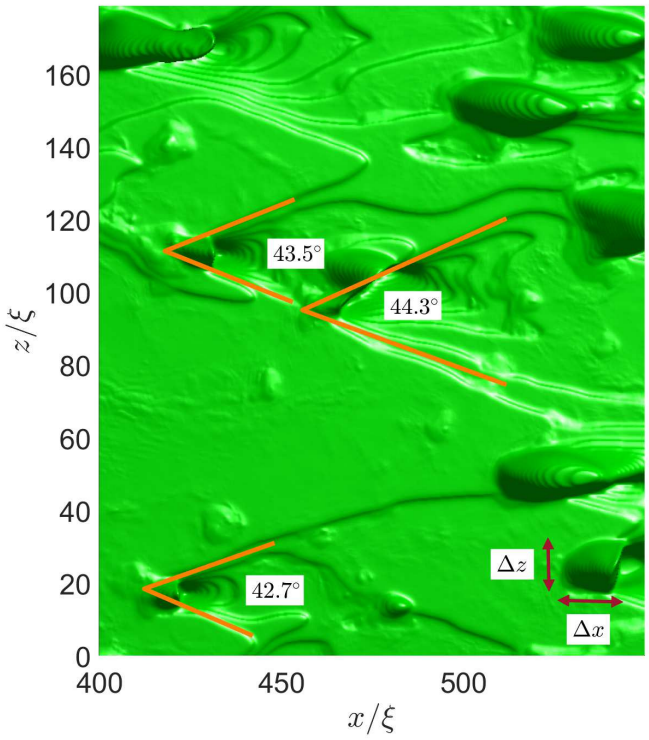

Suppl. Fig. 1: **A fractographic signature of crack front waves.** A zoom in on a few localized branching events originally presented in Fig. 3b and Fig. 3f in the manuscript (top view). For three localized branching events, the V-shaped tracks (see text for details) are marked and their opening angle 2γ is indicated. The latter, corresponding to $\gamma \simeq 21.75°$, is essentially the same for the three events. The localized branch width Δz and length Δx are illustrated for the localized branching event in the bottom-right corner. Results involving Δz and Δx are presented in Fig. 4b and the inset of Fig. 5 in the manuscript, and discussed therein.

C. Asymmetric localized branch profiles

Some experimental evidence indicates that micro-branches are asymmetric (with respect to the main crack plane), at least at not too high crack propagation velocities, e.g., see the middle panel (center) in Fig. 4c in [6]. That is, micro-branches in this regime do not appear to be formed in pairs that propagate predominantly symmetrically, but rather single micro-branches tend to form and either propagate upwards or downwards relative to the main crack plane. It has been experimentally shown that the micro-branches approximately follow a $y \sim x^{0.7}$ profile out of the crack plane ($y=0$, where x is the propagation direction).

Many of the localized branching events in our simulations, especially in the not too high velocities regime, are indeed asymmetric. That is, even if a pair of localized branches initially forms, the quenched disorder and/or the interaction with other out-of-plane structures break the up-down symmetry, resulting in a single dominant localized branch. In these situations, we expect the approximate $y \sim x^{0.7}$ profile — that emerges from the elastodynamic interaction of the localized branch with the main crack — to be observed in our case as well. This is indeed demonstrated in Fig. 2

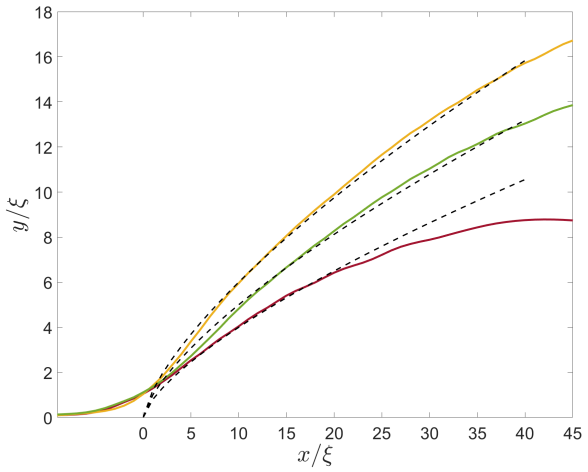

Suppl. Fig. 2: **The out-of-plane spatial profile of asymmetric localized branches.** Three examples of the $x-y$ profile of asymmetric localized branches (in the z direction) randomly selected from our simulations (and shifted such that they all overlap at their early stages of development). The dashed lines are guides to eye corresponding to $y \sim x^{0.7}$, as found experimentally (e.g., see Fig. 12 in [6] and Fig. 2 in [7]), each with a different amplitude.

D. 2D disordered materials

The most well developed dynamic fracture experiments in the quasi-2D limit, i.e., in very thin samples (small L_z), were performed on brittle polymeric gels [8, 9]. As discussed in the manuscript, both the 2D oscillatory instability [8] and the 2D tip-splitting instability [9] in these materials have been quantitatively understood as linear instabilities, without invoking finite quenched disorder. The physical origin of this observation may be either that the thin gel formation protocol (involving two confining glass plates with a gap of $\sim 150-200\,\mu$m [8]) suppresses the level of disorder or that the large nonlinear elastic zone near the crack front [9–11] effectively smooths out spatial fluctuations, or both. Nevertheless, in a broader scientific context not directly related to available experimental observations, it would be interesting to study the effect of finite quenched disorder on 2D crack dynamics within our flexible computational framework.

Our goal here is to calculate $\Gamma_{\rm 2D}(v,\sigma)$, i.e., the effective fracture energy in 2D disordered systems that feature quenched disorder of strength σ, with a spatial correlation length $R=10\xi$. Results for the homogeneous limit, $\Gamma_{\rm 2D}(v) = \Gamma_{\rm 2D}(v,\sigma=0)$, are presented in Fig. 2 in the manuscript (see also Eq. (1) therein). We generated a

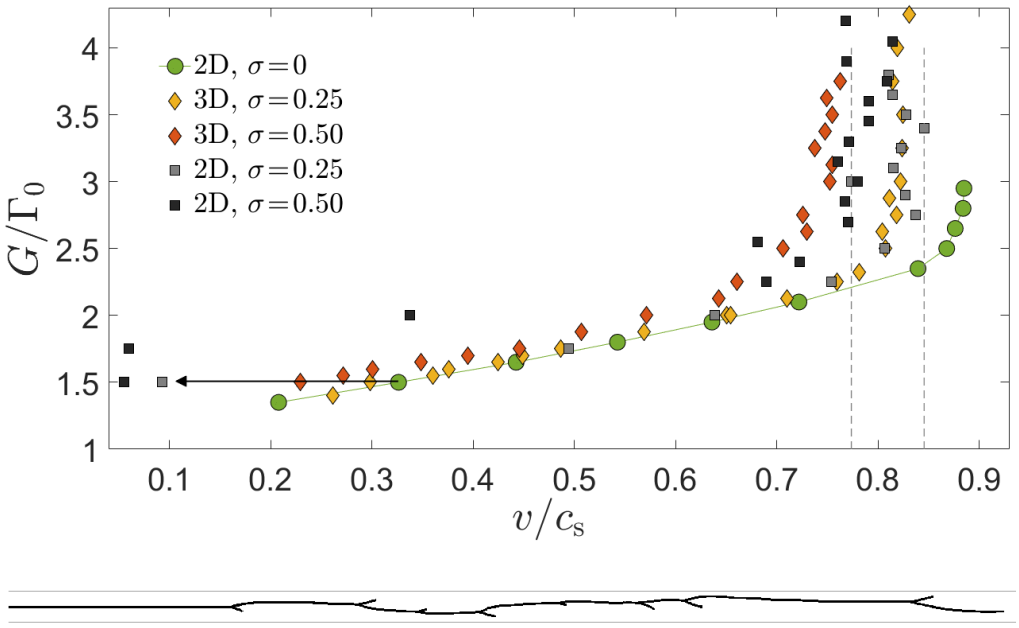

Suppl. Fig. 3: **Comparison of the crack driving force as a function of its propagation velocity in 2D and 3D, at various levels of disorder.** (Upper panel) Comparison between the normalized fracture energy in 2D and 3D, presenting G/Γ_0 vs. v/c_s. The results for a 2D homogeneous material, and for 3D materials with $\sigma=0.25$ and $\sigma=0.50$ (both with $R=10\xi$), are the same as in Fig. 2 in the manuscript (same symbols and colors, see legend). Results for 2D disordered materials are added (for $\sigma=0.25$ and $\sigma=0.50$, both with $R=10\xi$, see legend), and are discussed in the text. (Lower panel) The postmortem 2D crack pattern for $\sigma=0.25$ and $G/\Gamma_0=2.75$.

2D static fracture energy quenched disorder field, characterized by strength σ and $R=10\xi$, similarly to the 3D procedure. We have then driven cracks in 2D samples (i.e., $L_z=0$) of the same L_y as in 3D by various crack driving forces $G/\Gamma_0>1$, and allowed them to propagate over distances comparable to their 3D counterparts in the manuscript, until reaching an average steady state velocity v. The 2D $G(v)$ results for both $\sigma=0.25$ and $\sigma=0.50$ are presented in Fig. 3 (recall that $\Gamma_{\rm 2D}(v,\sigma)=G$ under steady-state propagation conditions). We also plot in Fig. 3 the 3D results already presented in Fig. 2 in the manuscript, along with the reference 2D homogeneous ($\sigma=0$) results (using the same symbols and colors, see legend).

Let us first compare the 2D $\sigma=0.25$ (grey squares) results to their 2D $\sigma=0$ (green circles) and 3D $\sigma=0.25$ (yellow diamonds) counterparts in Fig. 3. We identify three different regimes: (i) At small G/Γ_0 values, the 2D $\sigma=0.25$ results significantly deviate (see the leftmost grey square) from the 2D $\sigma=0$ results, in sharp contrast to the 3D $\sigma=0.25$ results. The deviation is highlighted by the left-pointing arrow, corresponding to $G/\Gamma_0=1.5$. The physical origin of this deviation is crack arrest, which is very probable for 2D cracks with $\sigma=0.25$ under this driving force, due to the encounter of large fracture energy fluctuations. This is in qualitative contrast to the corresponding 3D case, in which crack front degrees of freedom (along $L_z>0$) entirely eliminate crack arrest. We note that arrested cracks obviously do not correspond to steady state cracks of finite propagation velocity. In Fig. 3, we assign to arrested cracks an average velocity computed over the allocated simulation time (hence taking into account both the initial crack acceleration phase and the vanishing velocity of the arrested crack), and as such is quite arbitrary. Yet, our only goal was to highlight in the figure crack arrest by revealing a strong left deviation from the 2D $\sigma=0$ curve.

(ii) At intermediate G/Γ_0 values, crack arrest probability is small and the branching/tip-splitting probability is also small, hence the 2D $\sigma=0.25$ fracture energy essentially identifies with the homogeneous 2D fracture energy and with the 3D disordered one in this regime. (iii) For $G/\Gamma_0\geq 2.5$, $\Gamma_{\rm 2D}(v,\sigma)$ upward deviates from $\Gamma_{\rm 2D}(v)$, similarly to the deviation observed (and extensively discussed in the manuscript) for 3D disordered systems. The origin of the deviation is the interaction of the crack with fracture energy fluctuations and repeated branching/tip-splitting events, as illustrated in the crack morphology shown in the lower panel (for $G/\Gamma_0=2.75$ and $\sigma=0.25$), which generate extra fracture surfaces/dissipation. The main difference compared to 3D disordered systems is that a limiting velocity is less well defined in 2D, revealing a larger spread (see the two vertical dashed lines added to highlight the observed range of velocities in the large G/Γ_0 regime for $\sigma=0.25$), typically around a larger velocity compared to the 3D limiting one. In that sense,

2D crack dynamics appear to be less "self-averaging" over the quenched disorder compared to their 3D counterparts, while the overall trends are qualitatively similar.

The 2D results for $\sigma = 0.50$ are superimposed (black squares) and are generally similar, though crack arrest is more dominant and persists to larger G/Γ_0 values (the three leftmost black squares correspond to arrested cracks), and the deviation from the corresponding 3D limiting velocity is more pronounced (towards larger velocities). We note that the repeated branching/tip-splitting crack pattern presented in the lower panel of Fig. 3 bears some qualitative similarities to the crack pattern observed in ultra-thin amorphous carbon (see [12] and Fig. 5a therein), though the latter experiments did not achieve quasi-steady-state conditions and the fracture energy was not quantified. Overall, despite the various differences highlighted above, the emergence of a limiting velocity and the dynamic renormalization of the fracture energy due to the disorder-induced generation of extra fracture surface through branching appear to be qualitatively similar in 2D and 3D, although the associated crack patterns are significantly different.

II. Supplementary References

[1] E. Sharon, G. Cohen, and J. Fineberg, Crack front waves and the dynamics of a rapidly moving crack, Physical Review Letters **88**, 085503 (2002).

[2] J. Fineberg, E. Sharon, and G. Cohen, Crack front waves in dynamic fracture, International Journal of Fracture **121**, 55 (2003).

[3] A. Livne, G. Cohen, and J. Fineberg, Universality and hysteretic dynamics in rapid fracture, Physical Review Letters **94**, 224301 (2005).

[4] S. Das, Y. Lubomirsky, and E. Bouchbinder, Dynamics of crack front waves in three-dimensional material failure, Physical Review E **108**, L043002 (2023).

[5] M. Adda-Bedia, R. E. Arias, E. Bouchbinder, and E. Katzav, Dynamic stability of crack fronts: Out-of-plane corrugations, Physical Review Letters **110**, 014302 (2013).

[6] E. Sharon and J. Fineberg, Microbranching instability and the dynamic fracture of brittle materials, Physical Review B **54**, 7128 (1996).

[7] E. Sharon and J. Fineberg, Universal features of the microbranching instability in dynamic fracture, Philosophical Magazine B **78**, 243 (1998).

[8] A. Livne, O. Ben-David, and J. Fineberg, Oscillations in rapid fracture, Physical Review Letters **98**, 124301 (2007).

[9] Y. Lubomirsky, C.-H. Chen, A. Karma, and E. Bouchbinder, Universality and stability phase diagram of two-dimensional brittle fracture, Physical Review Letters **121**, 134301 (2018).

[10] C.-H. Chen, E. Bouchbinder, and A. Karma, Instability in dynamic fracture and the failure of the classical theory of cracks, Nature Physics **13**, 1186 (2017).

[11] A. Vasudevan, Y. Lubomirsky, C.-H. Chen, E. Bouchbinder, and A. Karma, Oscillatory and tip-splitting instabilities in 2D dynamic fracture: The roles of intrinsic material length and time scales, Journal of the Mechanics and Physics of Solids **151**, 104372 (2021).

[12] J. Yoon, Y. Jang, K. Kim, J. Kim, S. Son, and Z. Lee, In situ tensile and fracture behavior of monolithic ultra-thin amorphous carbon in TEM, Carbon **196**, 236 (2022).